Landslides
DOI 10.1007/s10346-018-0947-7
Received: 1 August 2017
Accepted: 4 January 2018

Luigi Borrelli · Mariantonetta Ciurleo · Giovanni Gullà

Shallow landslide susceptibility assessment in granitic rocks using GIS-based statistical methods: the contribution of the weathering grade map

Abstract Shallow landslides (i.e., slide, flow, and complex) are widespread around the world, affecting the soil mantle and upper regolith as a result of the weathering of granitic bedrock, and periodically cause enormous social and economic damages. Shallow landslide hazards are predominantly due to the scarcity of warning signs during the pre-failure stage, high velocities reached in the post-failure phase, and an increase in mobilized volumes caused by the entrapment of material in the downhill path of the phenomena. Owing to the abovementioned aspects, susceptibility assessment of shallow landslides in weathered granitic rocks is a relevant issue for land use planning and design purposes. This study proposes a three-step methodology for the susceptibility assessment of these phenomena. The methodology has been tested and validated at the 1:10,000 scale over a 30.4-km^2 area in southern Italy, where weathered granitic rocks are periodically affected by shallow landslides. This methodology is divided into three successive steps: step 1 consists of database creation, with an emphasis on the weathering grade map (including five weathering classes, from class II to class VI, each one characterized by comparable mechanical behavior), and steps 2 and 3 focus respectively on susceptibility map calibration and validation through statistical analyses. The area under the ROC curve (AUC) shows values ranging from 0.95 in step 2 (calibration) to 0.88 in step 3 (validation) and is a testament to the good overall predictive accuracy of the methodology. The obtained results demonstrate both the effectiveness and the consistency of the proposed methodology in performing susceptibility mapping of shallow landslides in weathered granitic rocks, as well as the important role played by the weathering grade map.

Keywords Granitic rocks · Weathering grade map · Shallow landslides · Susceptibility · Statistical analysis · Calabria (Italy)

Introduction

In a geological context, where weathered granitic rocks are widespread, the morphodynamic evolution of slopes and slope instability are strongly related to the intensity of weathering and features of weathering profiles (Durgin 1977; Ollier 1984, 1988; Chigira and Ito 1999; Le Pera and Sorriso-Valvo 2000; Whalley and Turkington 2001; Borrelli et al. 2014b; Borrelli and Gullà 2017). In particular, shallow landslides (SLs) in weathered granitic rocks are widespread around the world (Deere and Patton 1971; Durgin 1977; Chigira et al. 2011; Calcaterra and Parise 2010; Lee et al. 2002; Palacios et al. 2003; Lacerda 2007; Das et al. 2010). SLs are characterized by relatively shallow failure surfaces (typically 2–3 m depth) that affect the soil mantle and upper regolith (saprolitic, residual, and colluvial soils), originating from the weathering of bedrock through chemical decomposition and physical disintegration (Irfan and Dearman 1978). The petrographic and mineralogical changes linked to weathering processes (Le Pera et al. 2001; Perri et al. 2014; Scarciglia et al. 2016) affect almost all the engineering properties of rocks, and in most cases, these effects are unfavorable because they reduce both the strength and stability of rock masses (Lumb 1962; Fookes et al. 1971; Baynes and Dearman 1978; Irfan and Dearman 1978; Cascini and Gullà 1993; Gan and Fredlund 1996; Gullà et al. 2012). Because the weathering grade of granitic rocks reflects their engineering characteristics and performances (Chiu and Ng 2014), in the study of weathering-related shallow slope movements, it is necessary to focus on the production of specific geoengineering maps, where the goal is the subdivision, classification, and mapping of the weathering grade in outcrops through the observation of geologically distinctive characteristics, as well as qualitative and semi-quantitative engineering–geological tests (Borrelli et al. 2007, 2014b, 2015a).

SLs affecting granitic slopes have typical main characteristics, which are summarized as follows: (i) limited soil thickness, (ii) high-density distribution of the phenomena per unit area, (iii) rapid triggering and high-speed movement, (iv) lack of warning signs in the pre-failure stage (absence of evidence of incipient motion) and limited predictability, and (v) variable spatial trajectories of descent on the slope with a considerable probability of involving anthropogenic areas (especially infrastructure and/or other structures).

Owing to the scarcity of warning signs and the wide spatial distribution, SLs are difficult to monitor and, as a result, susceptibility assessments of SLs in weathered rocks may be simultaneously considered both the most effective approach to forecast these phenomena (Corominas et al. 2014) and a relevant issue for land use planning and design purposes.

Soeters and van Westen (1996), Cascini (2008), and Fell et al. (2008) classify the methods employed to derive landslide susceptibility as basic (or heuristic), intermediate (or statistical), and advanced (or deterministic), and propose a correlation among these methods, scales of analysis, and zoning purposes to define the respective three zoning levels: preliminary, intermediate, and advanced.

The basic methods are essentially based on topographic, geological, and geomorphological data; intermediate methods can be used if further details from the input data will be added, and statistical analysis-based procedures will be used (van Westen 1994; Carrara et al. 1995; Santacana et al. 2003; Calvello and Ciurleo 2016); finally, advanced methods require hydrogeological and geotechnical data and either deterministic or probabilistic procedures (Goodman and Shi 1985; Duncan 1992; Savage et al. 2004; Baum et al. 2005; Nadim et al. 2005; Cascini 2008; Cascini et al. 2015; Ciurleo et al. 2017).

In particular, the use of intermediate methods (statistical analyses) is recommended at a large scale (from 1:25,000 to 1:5000) and allows the achievement of an intermediate level of zoning (Fell et al. 2008).

Furthermore, within the literature that deals with landslide susceptibility and hazard assessment, few papers have focused on the relationship between landslide susceptibility and weathered rocks (Das et al. 2010; Kim et al. 2016; Padrones et al. 2017) and even fewer on the use of a weathering grade map in SL

Published online: 13 January 2018

susceptibility assessment (e.g., Sujatha et al. 2012). Because the weathering grade plays a key role as a predisposing factor to SL development (Tobe and Chigira 2006; Chigira et al. 2011), traditional geological and lithological maps are not sufficient for the determination and quantification of the weathering processes affecting granitic rocks. In this regard, the lack of understanding of the presence of different degrees of weathering (which implies different behavior in terms of physical properties, as well as in the hydrogeological setting) may lead to the wrong decisions and an overestimation of the susceptibility, hazard, and risk of SLs.

All that being considered, we propose a methodology based on statistical analyses at the 1:10,000 scale for application to a case study located in the Calabria region (Southern Italy), where weathered granitic rocks are widespread and affected by SLs.

The aim of this paper is to both identify the most relevant predisposing factors of SLs in weathered crystalline rocks and to quantify the role of a weathering grade map in shallow landslide susceptibility assessment by statistical analyses.

Materials and methods

Study area

The study area is located in southern Italy, in the Vibo Valentia Province of the Calabria region. It is bordered to NW by the Tyrrhenian Sea and to SE by the Monte Poro massif (Fig. 1). This area extends 30.4 km^2 and ranges in elevation from 0 to 711 m a.s.l. It is widely known for its scenic landscape and favorable climatic conditions, which have caused heavy exploitation of this coastal area, especially through tourism, which is the main source of income. The landscape of the study area shows a complex morphology that consists of narrow, elongated marine terraces (Tortorici et al. 2003) parallel to the coastline and it is bounded by well-developed inner edges. Narrow and fault-aligned valleys (e.g., Burmaria and Delle Grazie Torrents) dissect the topographic surface, producing steep slopes. The mean slope gradient ranges from 0 (marine terraces and coastal plain) to approximately 71° (at the borders of the main canyons).

Because of its geographic position, the study area is characterized by a highly variable climate with typically dry, subtropical summers. The annual rainfall values range between 300 and 600 mm (Ferrari et al. 2013).

This area was widely affected by different shallow landslide events (Antronico et al. 2004; Gullà et al. 2004; Borrelli and Gullà 2002), the most recent was the events which occurred in the winters between 2008 and 2010 (e.g., Gullà et al. 2009; Antronico et al. 2013; Borrelli et al. 2015a; Cascini et al. 2015; Ciurleo et al. 2016; Cascini et al. 2017), inducing damage to private property and infrastructure and causing considerable economic damages (Antronico et al. 2017; Ietto 2012).

Methodology

The proposed methodology is divided into three steps: step 1 consists of database creation; step 2 consists of the calibration of the statistical model and it ends with the production of a landslide susceptibility computational map; and step 3 consists of the validation of statistical analysis performed in the previous step (Fig. 2). At the end, the methodology provides a reliable shallow landslide susceptibility map at the 1:10,000 scale.

Step 1 includes the production of landslide inventories and geostructural and weathering grade maps.

Referring to landslide inventory, on the one hand, Fell et al. (2008) suggested mapping the landslide inventory at a scale larger than the susceptibility zoning map; on the other hand, Steger et al. (2017) highlighted the influence of systematically incomplete landslide inventories in statistical susceptibility models. In the present paper, different procedures (i.e., aerial photographs interpretation, visual inspection of digital orthophotos and Google Earth satellite images, multi-temporal field surveys) have been used to create two accurate landslide inventory maps (Brunsden 1985; Sato and Harp 2009; Guzzetti et al. 2012), referring to landslides recorded in the 2001–2005 and 2008–2011 time spans, respectively.

The 2001–2005 inventory is derived from combining the visual interpretation of color stereoscopic aerial photographs dated 2001 (at the 1:15,000 scale) and the analysis of Google Earth satellite images dated 29th May 2003, 4th June 2003, and 21st March 2005 to map the phenomena that occurred until 2005. The 2008–2011 landslide inventory map is obtained through the analysis of both color digital orthophotos (at the 1:5000 scale), dated 2008, and Google Earth satellite images, dated 2nd May 2010 and 10th April 2011.

In particular, to produce these inventories, the visual inspection of freely accessible multi-temporal Google Earth satellite images represented a useful tool to easily identify and map SLs on the basis of the morphological signatures left by phenomena (e.g., freshness of the shape, tone, and texture) on the ground surface (e.g., Borrelli et al. 2015a; Boardman 2016). The resolution of these images allowed the clear identification of landslides with sizes up to 2 m by positioning the screen for a completely vertical view from a height of 50 m.

The two landslide inventory maps have been validated by field checks performed in 2002, 2005, 2009, and 2010 (Borrelli and Gullà 2002; Gullà et al. 2004; Antronico et al. 2017).

Geological mapping and structural investigations were completed by aerial photo interpretation and field surveys to investigate the morphological evidence linked to tectonics, as well as to identify faults and rock types (Fig. 2). Subsequently, the study focused on the weathering grade survey completed via specific codified procedures (e.g., Borrelli et al. 2007) allowing us to distinguish (along road cuts, river valleys, and exposed sections) the different classes of weathered outcrops. The used criteria were suggested by Borrelli et al. (2015b, c) that subdivide the weathering grade into six classes: class I (fresh rock), class II (slightly weathered rock), class III (moderately weathered rock), class IV (highly weathered rock), class V (completely weathered rock), and class VI (residual and colluvial soils and detrital weathered material).

During the weathering field surveys, the main engineering geological features of the different weathering classes were obtained using both qualitative (e.g., rock color, degree of discoloration, rock fragments broken by hand and by hammer, sound emitted when the rock is struck by a geological hammer) and quantitative (e.g., Schmidt Hammer tests) criteria.

Finally, the acquired data allowed the preparation of the thematic maps at the 1:10,000 scale in a GIS environment (Fig. 2).

In step 2, the abovementioned thematic maps were expressed in raster format using 303.189 square grid cells as terrain computational units (TCUs), where a single cell size is equal to 10 × 10 m. In particular, referring to landslide inventories, in the case where a TCU is only partially interested in a landslide edge, the TCU was considered to completely belong to the landslide. In this step, a statistical method is used to assess the susceptibility to SLs in the

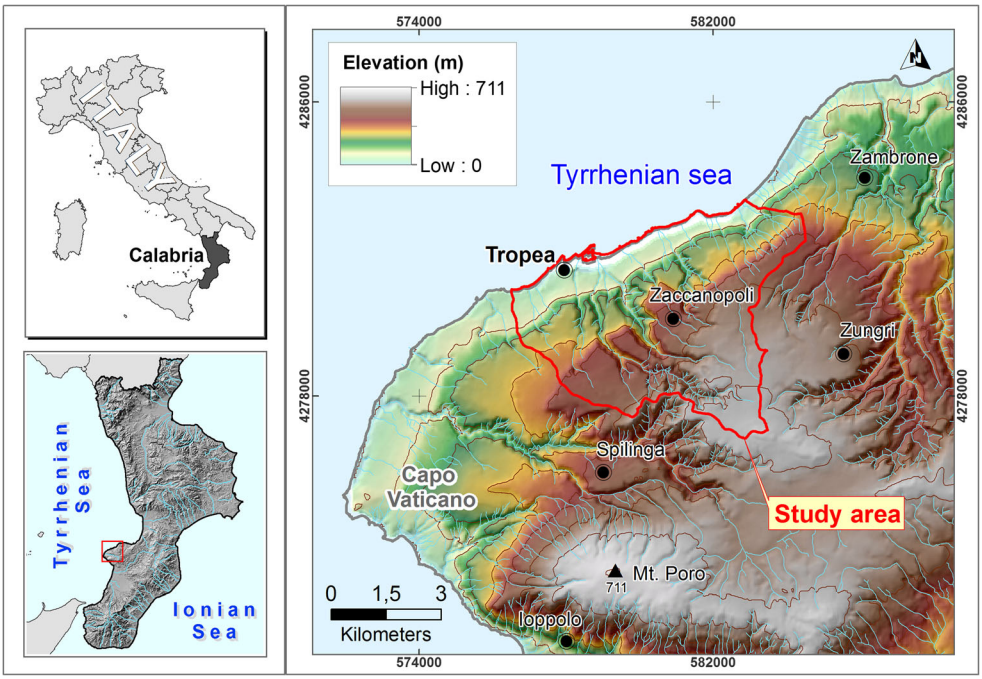

Fig. 1 Location of the study area

study area (Fig. 2), based on bivariate correlations (Tangestani 2009; Conforti et al. 2012; Ciurleo et al. 2016) between available independent variables (e.g., elevation map, slope gradient, weathering grade map) and a dichotomous dependent variable (dependent variable #1) derived from the landslide inventory dated 2001–2005. The categorical independent variables (geological and weathering grade maps) are divided into a number of classes directly correlated to the classification of the related thematic maps, while the numerical variables (e.g., elevation zone, slope gradient, slope curvature) are always divided in eight classes using the Jenks Natural Breaks algorithm (Jenks 1977). The statistical weight (assigned to each class *j* of each variable *Vi*) is computed by

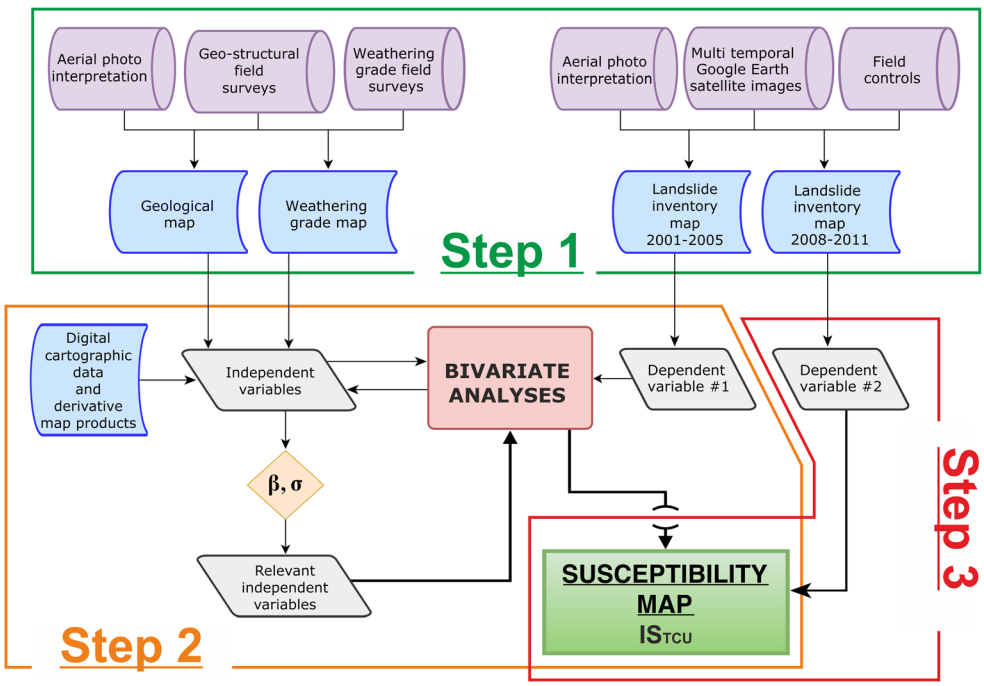

Fig. 2 Schematic flowchart of the methodology used for the SLs susceptibility assessment

the formula, originally proposed within the "information value method"(e.g., Yin and Yan 1988):

$$W_{ij} = \log\left(\frac{D_{ij}}{D^*}\right) = \log\left(\frac{F_{ij}/N_{ij}}{F_{tot}/N_{tot}}\right) \quad (1)$$

where W_{ij} is the weight assigned to class j of the independent variable Vi; D_{ij} is the density of landslides within class j of the independent variable Vi; D^* is the average density of landslides within the study area; F_{ij} is the number of terrain computational units (TCUs) with landslides belonging to class j of V_i; N_{ij} is the number of TCUs belonging to class j of Vi; F_{tot} is the total number of TCUs with landslides within the study area; and N_{tot} is the total number of TCUs within the study area.

High positive values of W_{ij} mean high probability that TCUs belonging to that class are affected by landslides; on the contrary, low negative values of W_{ij} mean low probability for TCUs belonging to a given class of a given variable to be affected by landslides. When landslides are not present in a given class of a given independent variable, Eq. 1 cannot be used to compute the weight values. In such cases, the class weight is herein set to a value equal to the closest negative integer inferior to the minimum computed weight for all classes of all variables (Ciurleo et al. 2016).

The performance assessment of the bivariate correlation between the independent and the dependent variables used herein is based on the values assumed by the bivariate success index (β_i) and the bivariate standard deviation index of the normalized weights (σ_i), defined by Ciurleo et al. (2016) as follows:

$$\beta_i = \frac{TPR_i}{FPR_i} = \frac{Sensitivity_i}{1-Specificity_i} = \frac{TP_i/(TP_i + FN_i)}{FP_i/(FP_i + TN_i)} \quad (2)$$

$$\sigma_i = \sqrt{\frac{\sum_{j=1}^{n}\left(W_{ij}^* - W_{-i}\right)^2}{n-1}} \quad (3)$$

where TPR_i is the true positive rate of the independent variable Vi (sensitivity); FPR_i is the false positive rate for Vi (1 − specificity); TP_i and FN_i represent the number of TCUs with phenomena belonging to the classes of the independent variable Vi, where the weight index respectively assumes a positive value (TP_i) or negative value (FN_i); and FP_i and TN_i are the number of TCUs without phenomena belonging to the classes of the independent variable Vi for which the weight index assumes a positive value (FP_i) or negative value (TN_i), respectively.

W_{ij}^* is the normalized value of the weight assigned to class j of the independent variable Vi (Ciurleo et al. 2016), W_i is the average value of the weights computed for each independent variable by Eq. 1, and n is the number of classes of the independent variable Vi.

The two indicators computed with Eqs. (2) and (3) have been proposed to select the independent variables that are relevant for a statistical analysis (Fig. 2).

Finally, the calibrated computational map (Fig. 2) is drawn by means of a multivariate susceptibility index, IS_{TCU}, computed according to the following formula:

$$IS_{TCU} = \sum_i W_{ik(i)} \quad (4)$$

where $W_{ik(i)}$ is the weight index of the relevant independent variable Vi, assigned to the TCU belonging to class $k(i)$ of that variable.

In step 3 (Fig. 2), the results obtained in the previous step in terms of IS_{TCU} have been validated by means of the landslide inventory dated 2008–2011 (dependent variable #2).

In step 2 (calibration) and step 3 (validation), the consistency of the obtained results is evaluated by means of area under the curve, AUC, of the receiver operating characteristic curves, ROC curves (Swets 1988).

Analyses and results

Step 1—database creation

Geomorphology, geology, and tectonics

The morphology of the study area, extending for 30.4 km², is strongly controlled by geology and tectonics (Ietto and Calcaterra 1988; Tortorici et al. 2003). The Quaternary tectonic uplift and related deepening of the hydrographic network increased the relief energy, giving rise to steep slopes and deeply cut valleys in the bedrock (Antronico et al. 2017). Slope gradient depends on the hardness of the different lithological units and, therefore, by the intensity of weathering processes that affected the granitoid rocks (Ietto et al. 2015).

The geological setting of this area (Fig. 3) mainly consists of an Ercinian Paleozoic crystalline basement (Monte Poro granitoid complex, Nicotera 1959), unconformably covered by Miocene transgressive siliciclastic-carbonate sediments (Amodio-Morelli et al., 1976; Ietto and Calcaterra 1988).

The granitoid rocks outcrop from the highest relief to the coastline and are widely exposed along a series of deeply incised valleys cut into the basement (e.g., Burmaria and Delle Grazie Torrents) (Fig. 3). They are mainly composed of coarse-grained tonalite with plagioclase phenocrysts, passing locally into granodiorite (Nicotera 1959; Perri et al. 2014).

The Miocene sequence that crops out discontinuously along the Tyrrhenian flank of the Monte Poro massif begins with the Tortonian ungraded quartz sands, evolving upwards into yellowish, poorly cemented sandstones (Nicotera 1959; Ietto and Calcaterra 1988; Papazzoni and Sirotti 1999; Ietto et al. 2015; Antronico et al. 2017). The thickness ranges from 20 to approximately 150 m.

Quaternary marine terraces (Tortorici et al. 2003), made up of siliciclastic sands and coarse sandstones or conglomerates (generally at the base of the sequence) with a fossiliferous content, unconformably cover the Tortonian marine sequence of the area (Fig. 3). The thickness of these terraces in the outcrops is generally lower than 10 m.

Holocene colluvial deposits derived from clastic slope-waste material are typically coarse-grained and immature, are widespread along the slope and at the valley bottom, and were brought there chiefly by sediment-gravity processes (Fig. 3).

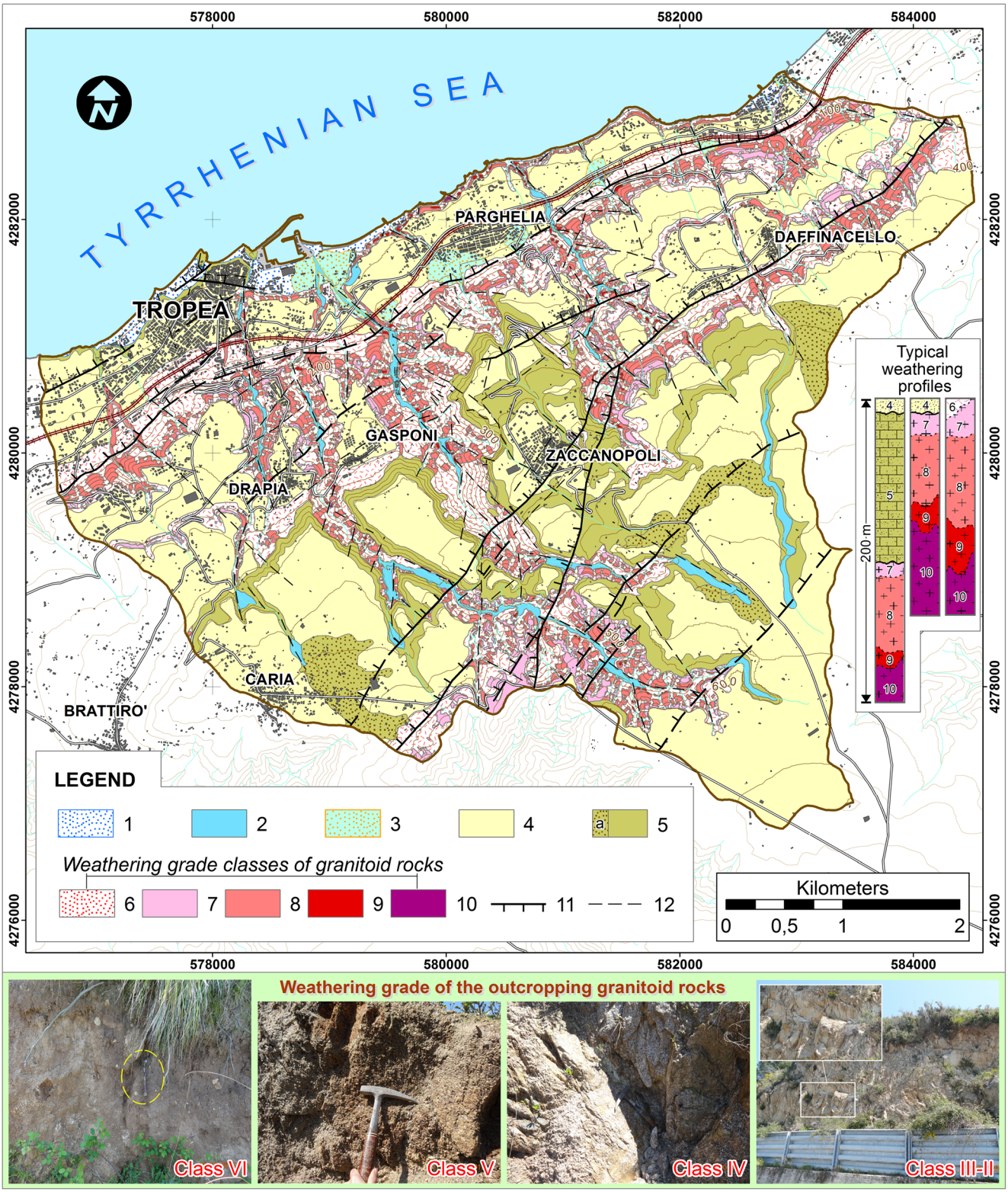

Fig. 3 Geostructural and weathering grade map of the study area (with schematized representation of three types of weathering profiles). Legend: (1) coastal and alluvial deposits (Holocene), (2) alluvial deposits (Holocene), (3) alluvial/debris fans (Holocene-Pleistocene Sup.), (4) Quaternary marine terraces composed of sands and coarse sandstones, (5) carbonate-cemented sandstones and (a) sands (Upper Miocene), (6) colluvial and residual soils (class VI), (7) completely weathered rocks (class V), (8) highly weathered rocks (class IV), (9) moderately weathered rocks (class III), (10) slightly weathered rocks (class II), (11) normal fault, (12) uncertain fault or main fractures

From a tectonic standpoint, two main NE–SW trending and NW-dipping normal faults, linked to a Quaternary tectonic extensional phase (Tortorici et al. 1995, 2003; Cucci and Tertulliani 2006; Borrelli et al. 2014a), characterize the study area (Fig. 3). The two major faults (i.e., Tropea and Zaccanopoli faults), arranged into a south-eastward, stepwise system, are clearly recognizable on a morphological basis and strongly control the morphology of the study area. These faults produce well-developed escarpments, with triangular and/or trapezoidal facets, and juxtapose the Neogene–Quaternary sediments with the underlying Paleozoic crystalline basement. Movements on these faults have produced several meters of vertical slip causing rock mass fracturing around them.

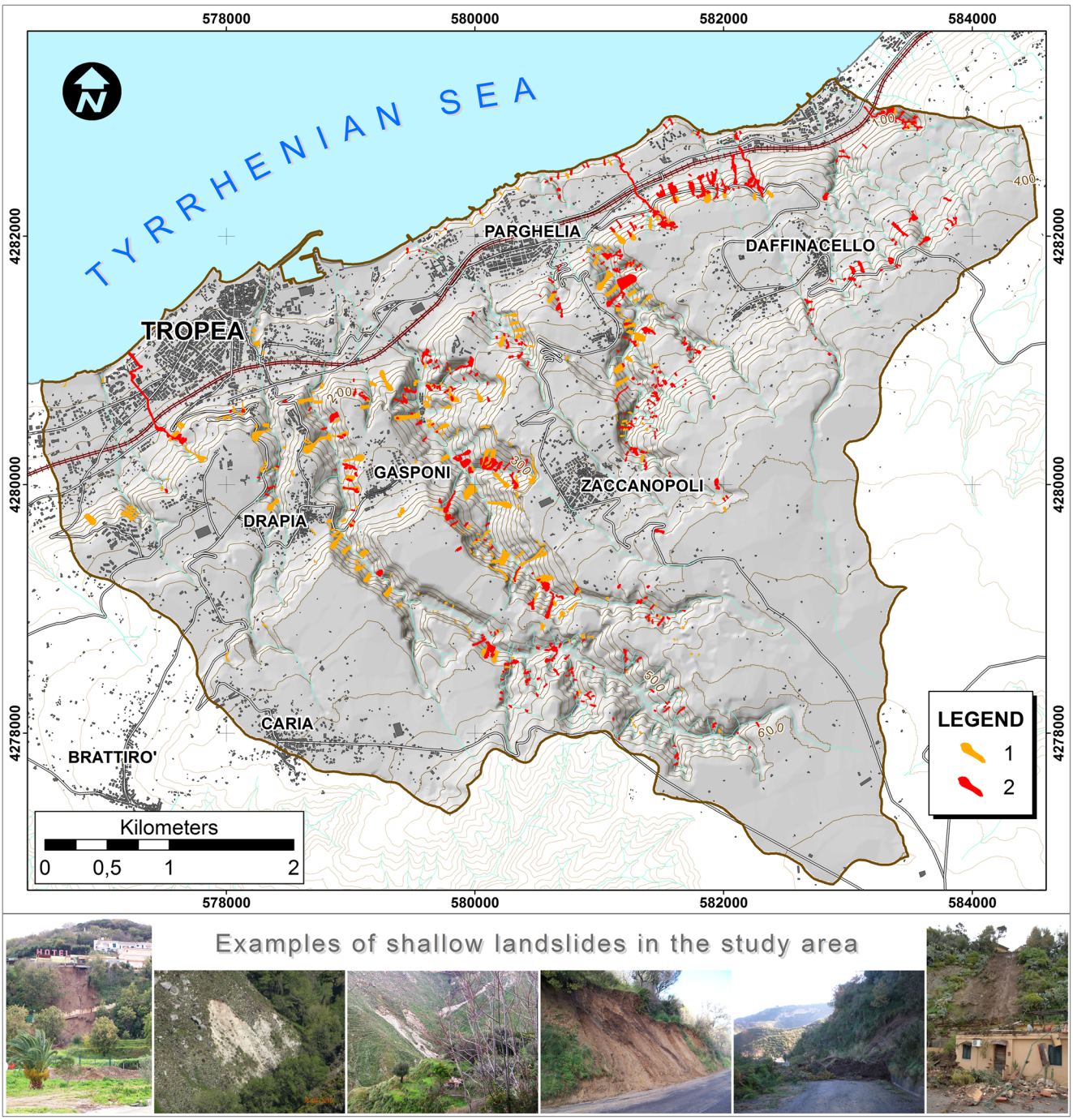

Fig. 4 Shallow landslide inventory map of the study area: (1) years 2001–2005, (2) years 2008–2011

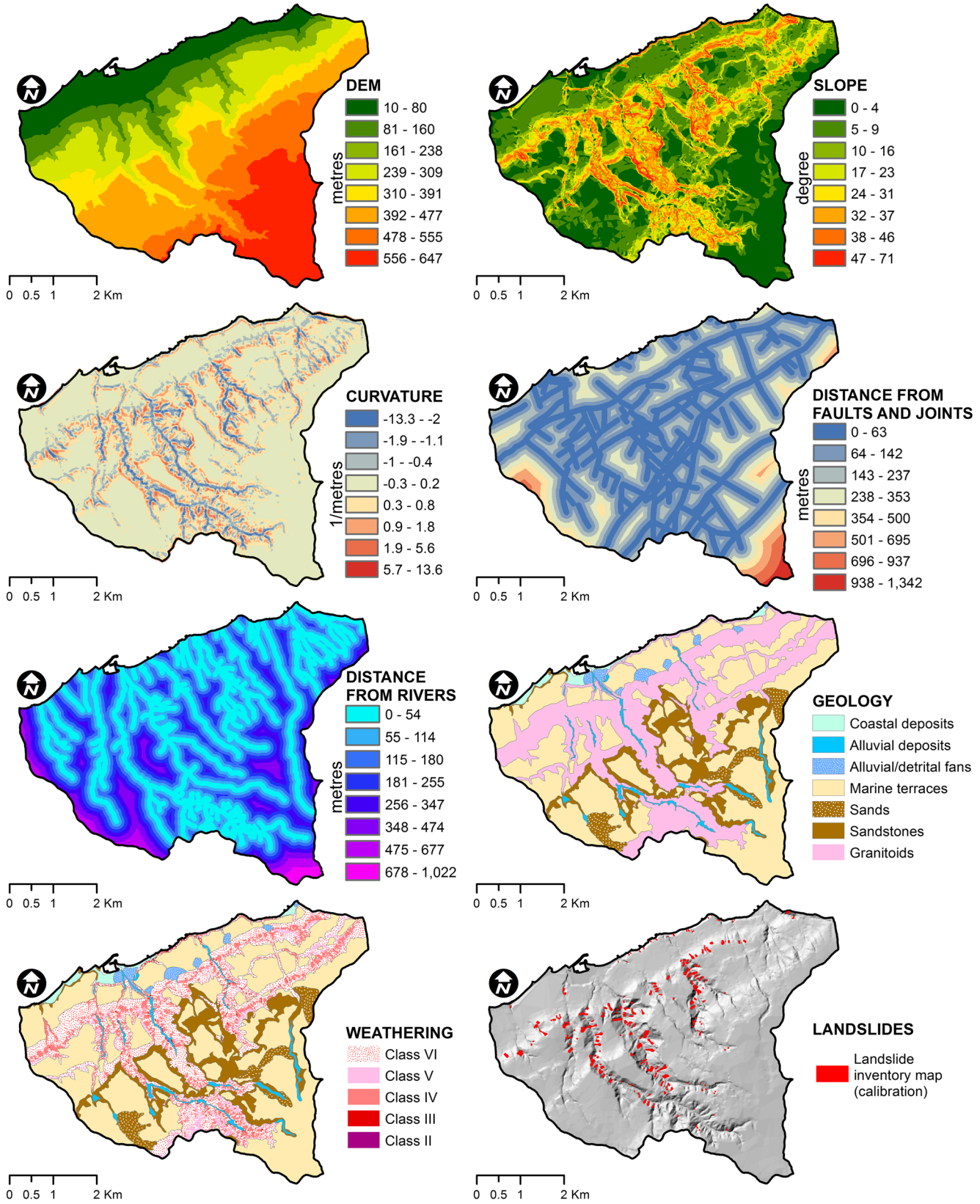

Fig. 5 Variables employed in the statistical analysis for the susceptibility assessment of SLs

Weathering features of granitoid rocks

The combination of tectonics and climate variation (between the Late Miocene and Pleistocene) plays an important role in the development of weathering processes in the study area (Borrelli and Gullà 2002; Gullà et al. 2004; Ietto and Ietto 2004; Perri et al. 2014; Ietto et al. 2015, 2017). Figure 3 provides a general comprehensive overview of the intensity and distribution of the rock mass weathering grades from class II (slightly weathered rock) to class VI (residual and colluvial soils).

Class II (slightly weathered rocks) and class III (moderately weathered rocks) are prevalent on outcrops along deeply incised streams and locally along road cuts, mainly at the valley bottom (Fig. 3). These rock masses show a pervasive discoloration near or around the discontinuities. The original texture and microstructure of the fresh rock are perfectly preserved, and the strength is comparable to that of the fresh rock (hard rock). Limited and isolated rock mass volumes can consist of class IV (highly weathered rock). The Schmidt Hammer rebound values range from > 50 for class II to 30–50 for class III.

Class IV (highly weathered rock) mainly outcrops along the middle-lower portion of the slopes and represents the most widespread class of weathering in the outcrops (Fig. 3). Class IV rock masses are completely discolored, but the original texture and microstructure of the fresh rock are still preserved. The strength is substantially reduced with respect to the original unweathered rock, and the Schmidt Hammer rebound values range from 10 to 30.

Class V (completely weathered rock or saprolitic soil) is widespread in the summit areas of the slope, mainly above 400 m a.s.l. (Fig. 3), where these rock masses can reach a maximum thickness of approximately 15 m. The rock masses are completely discolored, and the original texture and microstructure are present in relict form (Fig. 3). Class V shows a soil-like behavior (Schmidt Hammer rebound values ranging from 0 to 10), with a dominant granulometric fraction represented by sand and gravel and minor amounts of silt (Antronico et al. 2017).

Finally, class VI, which ranges in thickness from a few meters to decameters, is distributed along the slopes and at the valley bottoms (generally reaching a greater thickness inside the concave slope morphologies) and obscuring the underlying granitic substrate (Fig. 3). Class VI consists predominantly of soil that was reworked and transported by slope processes (colluvial deposits) and minor soil related to in situ weathering (residual soils) of a thickness that is not cartographable. In particular, colluvial deposits that occasionally exhibit distinct macrofabric and microfabric development, bedding structures, and evidence of distinct periods of accumulation are characterized by sand and gravel or sandy-silty chaotic terranes, including class III and class IV weathered centimetric rock fragments. Residual soils are represented by clayey silt to clayey sand with smooth-textured soil particles, and remnants of parent rock are not observed. The weathering class distribution is strongly controlled by tectonics (e.g., Borrelli and Gullà 2017). Normal fault planes vertically displaced the inherited weathered horizons, emplacing hanging-wall weathered rocks (classes VI and V) down to fresher footwall rocks (classes IV and III), which are mainly located within the fault-raised blocks (Fig. 3). Moreover, along the fault planes (i.e., within the fault zones), many different types of weathered rocks have been found, including variable thickness, severely deformed, and smashed and ground-up rocks.

Finally, all of the collected data indicate that the typical weathering profile is generally simple (sensu Brand and Phillipson 1985), and the weathering front (from class VI to class IV) is propagated in the granitic bedrock to a depth of 60 m (Fig. 3).

Multi-temporal SLs inventory map

The multi-temporal SLs inventory map (Fig. 4) shows 832 SLs and 34 areas affected by falls (274 SLs and 30 areas affected by falls relative to the 2001–2005 period and 558 SLs and 4 falls relative to the 2008–2011 period) of different type and size, with an average density of approximately 28 landslides/km^2.

In particular, the inventory map shows 594 complex landslides (i.e., slide-flows corresponding to 65% of the total area affected by SLs), 238 slides (32%), and 34 zones affected by falls (3%). The mapped landslides range in size from 25 to 13,000 m^2, for a total landslide area of 5.15×10^5 m^2, corresponding to 2% of the entire study area. This percentage rises to approximately 4%, excluding the flat morphologies (e.g., coastal plain and marine terraces).

Table 1 Classification of the independent variables employed in the statistical analysis

Class	V1 elevation zones (m)	V2 slope gradient (°)	V3 slope curvature (m^{-1})	V4 distance from faults and joints (m)	V5 distance from rivers (m)	V6 geology	V7 weathering
1	10 to 80	0 to 4	− 13.3 to − 2	0 to 63	0 to 54	Coastal deposits	Coastal deposits
2	81 to 160	5 to 9	− 1.9 to − 1.1	64 to 142	55 to 114	Alluvial deposits	Alluvial deposits
3	161 to 238	10 to 16	− 1 to − 0.4	143 to 237	115 to 180	Alluvial/detrital fans	Alluvial/detrital fans
4	239 to 309	17 to 23	− 0.3 to 0.2	238 to 353	181 to 255	Marine terraces	Marine terraces
5	310 to 391	24 to 31	0.3 to 0.8	354 to 500	256 to 347	Sands	Sands
6	392 to 477	32 to 37	0.9 to 1.8	501 to 695	348 to 474	Sandstones	Sandstones
7	478 to 555	38 to 46	1.9 to 5.6	696 to 937	475 to 677	Granitoids	Class VI
8	556 to 647	47 to 71	5.7 to 13.6	938 to 1342	678 to 1022		Class V
9							Class IV
10							Class III
11							Class II

Table 2 Weights assigned to the independent variables

Weights	V1	V2	V3	V4	V5	V6	V7
Wi1	− 0.64	− 1.60	0.61	0.25	0.23	− 3.00	− 3.00
Wi2	0.40	− 1.67	0.67	0.05	0.15	0.14	0.14
Wi3	0.72	− 0.75	0.51	− 0.54	− 0.22	− 3.00	− 3.00
Wi4	0.08	− 0.02	0.21	− 1.11	− 0.77	− 2.23	− 2.23
Wi5	0.01	0.37	− 0.55	− 3.00	− 0.67	− 3.00	− 3.00
Wi6	− 0.70	0.59	0.01	− 3.00	− 1.49	− 0.59	− 0.59
Wi7	− 1.17	0.71	0.13	− 3.00	− 3.00	0.45	0.61
Wi8	− 2.31	0.65	− 0.07	− 3.00	− 3.00		− 1.89
Wi9							− 3.00
Wi10							− 0.59
Wi11							− 3.00

SLs are distributed over the entire area, with a marked concentration along the main river valleys (Fig. 4). They occur prevalently on steep slopes, either isolated or clustered in groups of several failures, and mainly affecting low-order drainage channels (within morphological hollows) and minor open slopes with an average gradient of approximately 38°.

Most of the SLs started as debris slides where the material was completely mobilized, leaving empty scarps (detachment zones or source areas), and evolved into debris flows depending on local morphological conditions (Esposito et al. 2012; Borrelli et al. 2015a). During the movement, the landslide masses incorporated large boulders, organic debris (trees and bushes, etc.), and anthropogenic material through the erosion of land cover along the slopes and in the channels (often coinciding with drainage lines), increasing their erosive power, and sometimes, affecting cultivation, structures, and infrastructure (Ietto 2012; Antronico et al. 2017).

SLs are usually small to medium in size, with widths ranging from 5 to 80 m and lengths ranging from 5 to 200 m, and they typically affect the upper portions of the granitoid weathering profile, enclosing all of the soil mantle material, including saprolite, residual soil (paleosol and modern soil), and colluvium (Fairbridge 1968). The sliding surfaces of SLs are shallower than 5 m and are most commonly 2–3 m in depth (e.g., Borrelli et al. 2012; Ciurleo et al. 2016; Gioffrè et al. 2016).

In most cases, the slip surfaces developed within the colluvial cover or coincided with the zone of contact between the upper regolith horizon (class VI and V) and the bedrock (class IV and III). In some cases, the landslide surfaces are found at the boundary between classes VI and V or, more rarely, directly within the saprolitic rock (class V).

Step 2 and 3—statistical analyses

The dichotomous dependent variables have been derived from two multi-temporal shallow landslide inventories, which occurred in 2001–2005 and 2008–2011, respectively. The first inventory, used in the calibration phase (step 2), reports 274 SLs (slides and slide-flows) covering 2779 TCUs of the test area, while the second inventory, used in the validation phase (step 3), reports 558 phenomena (slides and slide-flows) covering 2681 TCUs.

The independent variables used in the analysis (Fig. 5, Table 1) are as follows: elevation zones (*V1*); slope gradient (*V2*); slope curvature (*V3*); distance from faults and joints (*V4*); distance from river networks (*V5*); geology (*V6*); and weathering (*V7*). All of the variables have been classified according to a natural breaks criterion that employs eight classes, except for geology and weathering (*V6* and *V7*), which have been divided into seven and eleven classes, respectively, following the classification reported in the employed thematic maps. The values of the statistics used to select the independent variables are reported in Tables 2 and 3, which respectively show the values of the statistical weights W_{ij} (Eq. 1) and the values assumed by the indexes β_i and σ_i (Eqs. 2 and 3).

Table 3 Values of parameters and indexes used to select the independent variables relevant for the statistical analysis

Variables	TN_i	TP_i	FN_i	FP_i	TPR_i (%)	FPR_i (%)	β_i	σ_i	Relevant
V1	179,088	2581	216	121,304	92.3	40.4	2.29	1.05	Yes
V2	230,456	2451	346	69,936	87.6	23.3	3.76	1.70	Yes
V3	171,668	2314	483	128,724	82.7	42.9	1.93	0.89	Yes
V4	109,644	2627	170	190,748	93.9	63.5	1.48	0.57	No
V5	136,934	2386	411	163,458	85.3	54.4	1.57	0.44	No
V6	195,429	2714	83	104,963	97.0	34.9	2.78	2.86	Yes
V7	227,319	2712	85	73,073	97.0	24.3	3.99	3.56	Yes

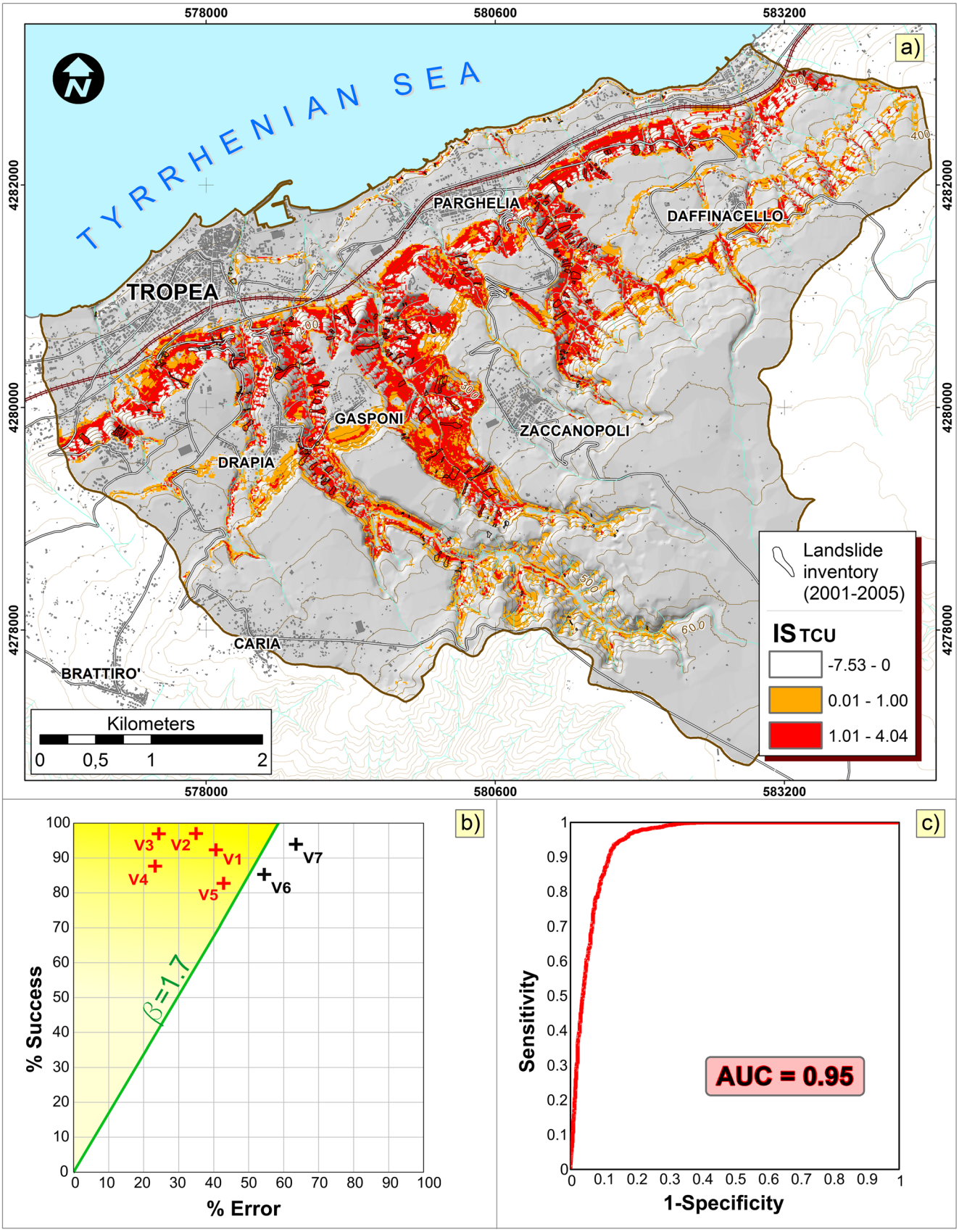

Fig. 6 Results of the statistical analysis: (a) computational landslide susceptibility map; (b) graphical representation of the TPR and FPR values of the independent variables employed in the analysis (V1, V2, V3, V7); (c) receiver operating characteristic curve

Table 2 shows that the overall maximum weight is attributed to class III of variable *V1* and class VII of *V2* ($W_{13} = 0.72$ and $W_{27} = 0.71$), which corresponds to an elevation zone from 160.51 to 238.32 m a.s.l. and a slope gradient ranging from 37.30° to 45.64°. High weights computed for variables *V3*, *V6*, and *V7* are equal to $W_{32} = 0.67$, $W_{67} = 0.45$, and $W_{77} = 0.61$, respectively.

Variables *V6* (geology) and *V7* (weathering) showed only two positive weights in both cases for classes II and VII. For both variables, class II, corresponding to alluvial deposits, assumes a weight of $W_{62} = W_{72} = 0.14$, while class VII, which corresponds to granitoid for *V6* and granitoid of class VI for *V7*, assumes a value equal to $W_{67} = 0.45$ and $W_{77} = 0.61$. Most of the classes of variables

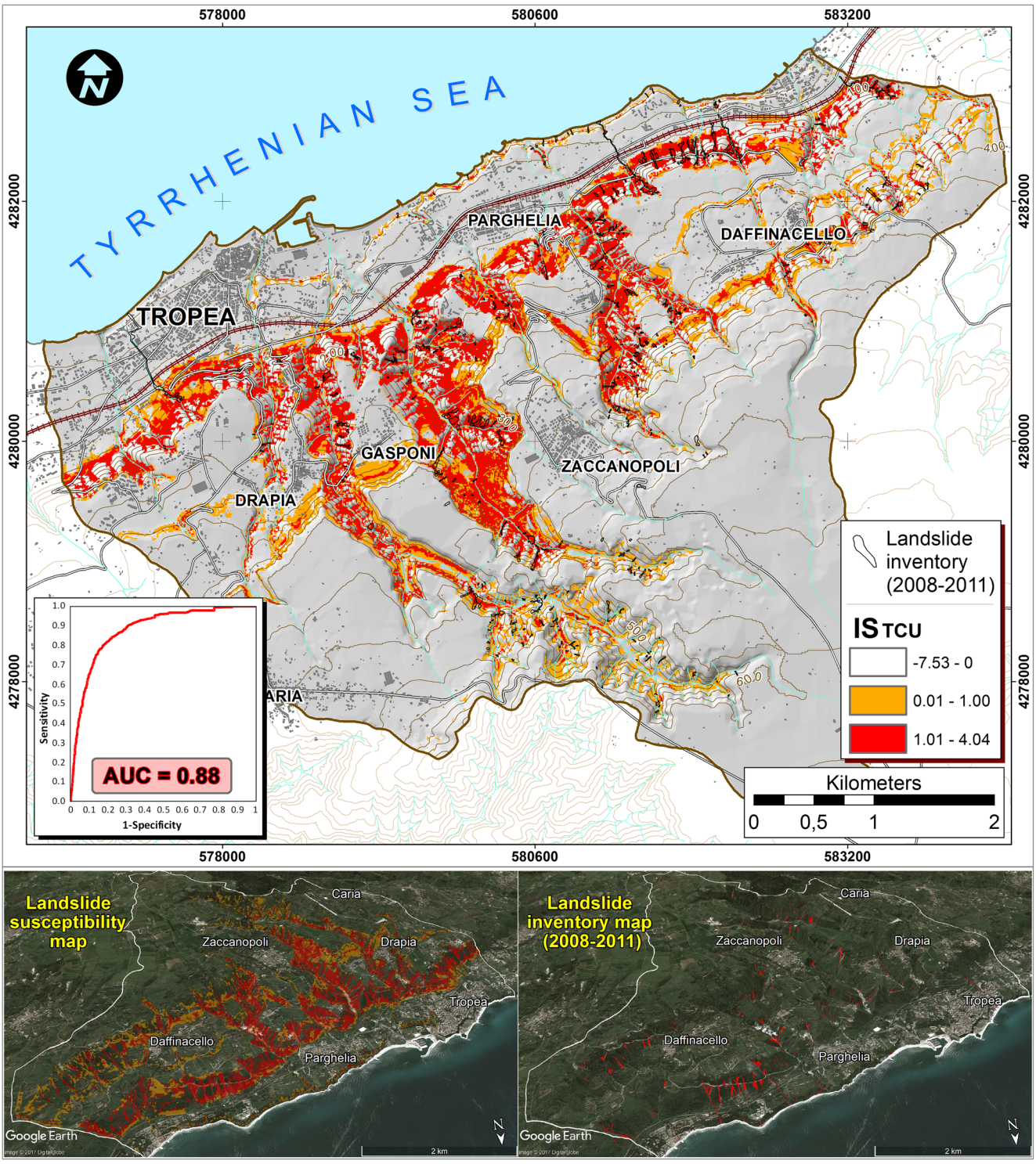

Fig. 7 Model validation of the susceptibility map

V6 and *V7* presented weight values lower than − 1.00, allowing for the identification of the strong correlation between the territory classified within those classes and the absence of SLs.

The lowest value computed in the analysis is − 2.31, corresponding to class VIII of variable *V1*, while the value of − 3.00, reported in Table 2, is imposed (not computed) by the user as the closest negative integer inferior to the minimum computed weight for all classes of all variables (Ciurleo et al. 2016).

The independent variables defined as relevant for the analysis (*V1*, *V2*, *V3*, *V6*, and *V7*) are identified by the values assumed by β_i (Eq. (2)) and σ_i (Eq. (3)).

According to Ciurleo et al. (2016), only the variables for which the two indexes assume values higher than 1.7 for β_i and 0.4 for σ_i are defined as relevant. Table 3 also reports the number of grid cells included in TP_i, FN_i, FP_i, and TN_i for each variable, in terms of the 2 × 2 contingency table, and the values of TPR_i, FPR_i used to compute the bivariate success index.

Following the values assumed for β_i and σ_i, variables *V6* and *V7* were considered relevant for the analysis, and both variables presented a value of TPR_i equal to 97%, while the value of FPR_i is equal to 34.9% for *V6* (geology) and decreases to 24.3% for *V7* (weathering grade map). Because the two variables can be considered representative of the same aspect, the weathering grade map, showing the lower value of FRP_i, is elected to be used with *V1*, *V2*, and *V3* in the computation of the multivariate susceptibility index IS_{TCU}.

Three susceptibility descriptors including low susceptibility $IS_{TCU} \leq 0$, medium susceptibility for $0 < IS_{TCU} \leq 1$, and high susceptibility for $IS_{TCU} > 1$ were used in the analysis (Fig. 6). It is worth highlighting that the high value assumed by the AUC of the ROC curve is equal to 0.95, testifying to the success of the analysis.

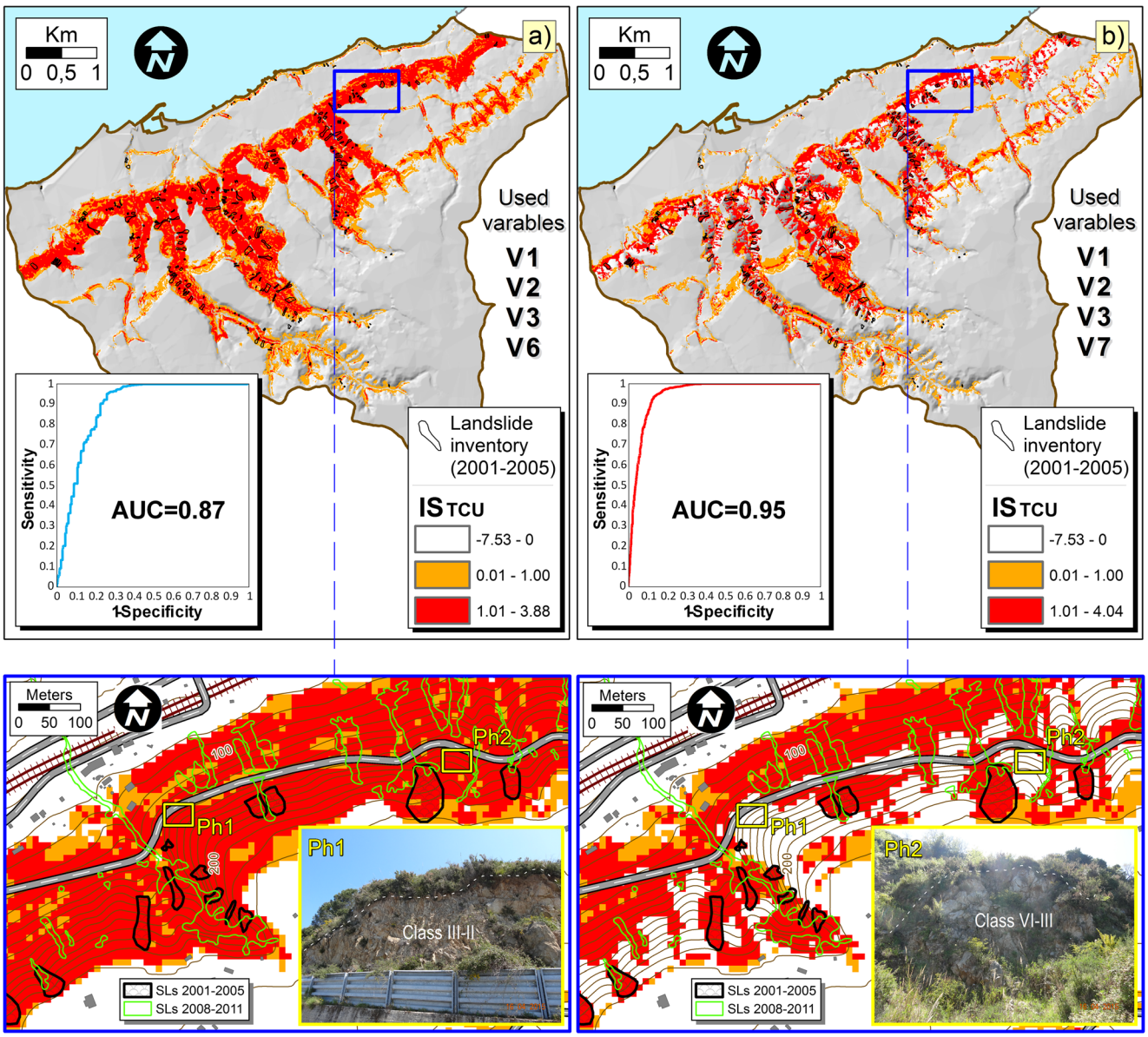

Fig. 8 Comparison between two susceptibility maps, receiver operating characteristic curves and the different results obtained for the same area. (a) Map obtained considering relevant independent variables *V1*, *V2*, *V3*, *V6*; (b) computational susceptibility map obtained considering relevant independent variables *V1*, *V2*, *V3*, *V7*

In step 3 (validation phase), considering the landslide inventory dated 2008–2011, the computed results showed a value of AUC equal to 0.88, a further testament to the consistency of the obtained results (Fig. 7).

Overall, 88% of landslides mapped from 2001 to 2011 fall within medium-high susceptible areas (i.e., $IS_{TCU} > 0$), and approximately 18% of the study area presents $IS_{TCU} > 0$.

Discussion

Landslide susceptibility can be assessed using different methods (heuristic, statistical, and deterministic) at different scales (small, medium, and large scale) to define three zoning levels: preliminary, intermediate, and advanced (Fell et al. 2008). Independent of the adopted methods and zoning levels, it is worth highlighting that good results in susceptibility zoning depend on the characteristics of the phenomena (typology, area and/or volume, etc.), the quality and accuracy of the available data within the area to be zoned, and the know-how and expertise of the analysts (Cascini 2008; Guzzetti et al. 2012).

Following Fell et al. (2008), the landslide inventory is the key parameter for susceptibility zoning, especially when it is prepared at a scale larger than the final susceptibility map. In this paper, we have used different procedures (aerial photographs interpretation, visual inspection of orthophotos and multi-temporal Google Earth satellite images) combined with multi-temporal field surveys to obtain a complete and accurate multi-temporal landslide inventory.

Moreover, the level and quality of susceptibility zoning also depends on the understanding of the role played by the predisposing factors of landslides (Cascini 2008). In this regard, it is important to underline that SLs that occurred in the study area involve soil-like rocks (i.e., class VI and minor class V), formed through the weathering of the granitoid bedrock. Weathering processes progressively worsen the geomechanical properties of the involved rock masses, favoring the development of an unconsolidated mantle of completely weathered rocks and soil materials; the mechanical changes observed in the advanced stages of weathering (particularly from class IV to class VI) are generally associated with both an increase of weathering products at the microscale (e.g., sericite, clay minerals, Fe-oxides, etc.), and the progressive formation of voids and fractures (Borrelli et al. 2014b, 2015b; Perri et al. 2014; Scarciglia et al. 2016). Gravitational forces acting on these disaggregated materials (i.e., saprolitic and residual soils) cause them to move down and accumulate along the slopes, forming colluvial deposits. Colluvial deposits are randomly widespread in the study area, reach a greater thickness inside the topographic depressions, and are related to very active morphodynamic processes.

The widespread presence of soil-like rocks produced by weathering constitutes a relevant predisposing factor to SLs, commonly characterized by predominantly translational slides, and in some cases rotational slides, often followed by a flow of the disturbed mass (Turner 1996; Gioffrè et al. 2016). In most cases, the slip surfaces (generally < 3 m) develop within the colluvial cover or coincide with the zone of contact between the upper regolith horizon (class VI and V) and the bedrock (class IV and III); although, in some cases, the landslide surfaces are found at the boundary between class VI and class V or, more rarely, are found directly within the saprolitic rock (class V).

Since the weathering grade of the granitic rocks reflects their engineering characteristics and performances (Heidari et al. 2011; Chiu and Ng 2014), the susceptibility assessment of SLs requires the production of a weathering grade map as a basic element and starting point, in addition to the classic geostructural map.

The role of the weathering grade as a predisposing factor to SLs is strongly confirmed by statistical analyses. The obtained results show that independent variables, identified as the most relevant predisposing factors of SLs on the basis of the statistical indicators β_i and σ_i, were as follows: elevation zone, slope gradient, slope curvature, geology, and weathering grade map (Table 3). The first four variables were considered to be relevant variables by other authors as well (Kayastha et al. 2013; Bui et al. 2016; Ciurleo et al. 2016), while the variable weathering grade is contemplated in only a few papers (e.g., Sujatha et al. 2012; Bui et al. 2016). This aspect can lead to incorrect landslide susceptibility analyses since the analyzed phenomena, as mentioned above, prevalently involve the upper part of the granitoid weathering profile (classes VI and V), which is not distinguished in a classic geological map. In this regard, referring to geology, the results of statistical analyses showed a true positive rate TPR_i equal to 97% (as weathering grade) but a value of a false positive rate FPR_i = 34.9%, which is appreciably higher than that computed for weathering (FPR_i = 24.3%). Furthermore, to stress the relevance of the weathering grade variable, Fig. 8 shows the comparison between two computational susceptibility maps. The first (Fig. 8a) was obtained considering relevant independent variables *V1* (elevation zone), *V2* (slope gradient), *V3* (slope curvature), and *V6* (geology), and the second (Figs. 6, 7, 8b) was obtained considering *V1* (elevation zone), *V2* (slope gradient), *V3* (slope curvature), and *V7* (weathering grade). In the first case (Fig. 8a), the map shows that approximately 27% of the study area has a medium-high susceptibility to SLs ($IS_{TCU} > 0$) and an AUC value of 0.87. In the second case (Figs. 6, 7, 8b), the computational susceptibility map shows that only 18% of the study area presents $IS_{TCU} > 0$, and the AUC of the ROC curve equals 0.95 (Fig. 8b).

Fressard et al. (2014), quoting Metz (1978), defined the following five classes of accuracy using the parameter AUC of a ROC curve: fail accuracy, for AUC values from 0.5 to 0.6; poor accuracy, for AUC values from 0.6 to 0.7; fair accuracy, for AUC values from 0.7 to 0.8; good accuracy for AUC values from 0.8 to 0.9; and excellent accuracy for AUC values from 0.9 to 1.0. Based on the previous statements, in the present analysis, an AUC = 0.87 indicates a good accuracy of the model, but excellent accuracy can be reached only by overcoming the threshold of AUC = 0.9, which is only possible by introducing the variable weathering grade map (AUC = 0.95).

Furthermore, two zooms in Fig. 8 highlight that where rocks outcrop (from highly to slightly weathered rocks), and SLs of the slide type cannot occur, the first map (Fig. 8a) shows a high susceptibility, while the second (Fig. 8b) shows a non-susceptible descriptor. The consistency of the obtained results is ascribed to the ability of the model to reduce the overestimation areas (Fig. 8a, b and respectively zooms), as well as to the capability of the map to forecast the phenomena that occurred from 2008 to 2011 (shallow landslide inventory used in step 3), as seen in the zoom of Fig. 8b and the AUC value equal to 0.88 in step 3 (Fig. 7).

To stress the relevance of the results obtained in this study, it is important to highlight that within the literature dealing with landslide susceptibility and hazard assessment, few analyses report AUC values higher than 0.9 (e.g., Lee et al. 2008; Bui et al. 2012; Marjanović 2013; Nefeslioglu et al. 2008; Ciurleo et al. 2016). However, when dealing with weathered rocks, even fewer analyses report the weathering grade map as input data (e.g., Cascini 2008;

Sujatha et al. 2012); consequently, landslide susceptibility is often overestimated (as reported in Fig. 8 and relative zooms) and, in some cases, not confidently usable in practice because this would lead to an unrealistic assessment of the risk related to these phenomena.

Conclusion

The paper reported a three-step methodology to produce a shallow landslide susceptibility map and evaluate the consistency of the results. The study area is characterized by widespread granitic rocks affected by intense weathering processes (particularly classes V and VI) that significantly reduce the rock strength and facilitate shallow slope failures.

After creation of the database (step 1), the "information value method" is implemented at the 1:10,000 scale using two dichotomous dependent variables (landslide inventories, for the periods of 2001–2005 and 2008–2011) to obtain and validate the computational landslide map (steps 2 and 3).

The three-step methodology allowed us to obtain an intermediate zoning level by statistical analyses without producing misleading results. This is due to a deep understanding of the role played by the predisposing factors of landslides. Indeed, the obtained results highlighted the key role played by the weathering grade map that combined with elevation, slope gradient, and slope curvature allowed us to obtain a value of the AUC of the ROC curve equal to 0.95 in the calibration phase (step 2), instead of 0.87 obtained when considering the geological map.

In summary, this study allowed us to (i) quantitatively define the role played by predisposing factors, (ii) identify the relevance of the weathering grade map that improves the quality of the obtained results and reduces the overestimation affecting the analyses when a classic geological map is considered, and (iii) achieve good results in the validation phase (step 3), with an AUC value equal to 0.88.

In conclusion, the excellent level of accuracy and the predictive efficiency of the model strongly suggest the production of a weathering grade map, which can be obtained through rapid techniques based on the observation of distinctive geological characteristics and simple qualitative and semi-quantitative index tests. This map should be considered a starting point for statistical analyses in contexts where weathered igneous rocks outcrop.

As a final remark, it is worth stating that the obtained susceptibility map may be employed for hazard and risk assessment to correctly manage land use and plan landslide risk reduction countermeasures whose effectiveness will also be increased through landslide typifying.

Acknowledgements

This work was conducted under the Project DTA.AD003.077.001 "Tipizzazione di eventi di dissesto idrogeologico" of the CNR Department of "Scienze del Sistema Terra e Tecnologie per l'Ambiente."

References

Amodio-Morelli L, Bonardi G, Colonna V, Dietrich D, Giunta G, Ippolito F, Liguori V, Lorenzoni S, Paglionico A, Perrone V, Piccarreta G, Russo M, Scandone P, Zanettin-Lorenzoni E, Zuppetta A (1976) L'Arco Calabro-Peloritano nell'orogene appennino-maghrebide. Mem Soc Geol Ital 17:1–60

Antronico L, Gullà G, Borrelli L (2004) Shallow instabilities for sliding flow: regional influence and area affects. In: Proc International Symposium on Landslide, June 28–July 2 2004, Rio de Janeiro. doi: https://doi.org/10.1201/b16816-197

Antronico L, Borrelli L, Coscarelli R, Pasqua AA, Petrucci O, Gullà G (2013) Slope movements induced by rainfalls damaging an urban area: the Catanzaro case study (Calabria, southern Italy). Landslides 10(6):801–814. https://doi.org/10.1007/s10346-013-0431-3

Antronico L, Borrelli L, Coscarelli R (2017) Recent damaging events on alluvial fans along a stretch of the Tyrrhenian coast of Calabria (southern Italy). Bull Eng Geol Environ 76(4):1399–1416. https://doi.org/10.1007/s10064-016-0922-2

Baum RL, Coe JA, Godt JW, Harp EL, Reid ME, Savage WZ, Schulz WH, Brien DL, Chleborad AF, McKenna JP, Michael JA (2005) Regional landslide hazard assessment for Seattle, Washington, USA. Landslides 2(4):266–279. https://doi.org/10.1007/s10346-005-0023-y

Baynes FJ, Dearman WR (1978) The relationship between the microfabric and the engineering properties of weathered granite. Bull Int Assoc Eng Geol 18(1):191–197. https://doi.org/10.1007/BF02635370

Boardman J (2016) The value of Google Earth™ for erosion mapping. Catena 143:123–127. https://doi.org/10.1016/j.catena.2016.03.031

Borrelli L, Gullà G (2002) Condizioni di alterazione nell'area a monte di Tropea (Calabria, Italia). CNR-IRPI Internal Report n 589

Borrelli L, Gullà G (2017) Tectonic constraints on a deep-seated rock slide in weathered crystalline rocks. Geomorphology 290:288–316. https://doi.org/10.1016/j.geomorph.2017.04.025

Borrelli L, Greco R, Gullà G (2007) Weathering grade of rock masses as a predisposing factor to slope instabilities: reconnaissance and control procedure. Geomorphology 87(3):158–175. https://doi.org/10.1016/j.geomorph.2006.03.031

Borrelli L, Gioffrè D, Gullà G, Moraci N (2012) Susceptibility to shallow and rapid landslides in ground alteration: a possible contribution of propagation modeling. Rend Online Soc Geol Ital 21:534–536

Borrelli L, Antronico L, Gullà G, Sorriso-Valvo GM (2014a) Geology, geomorphology and dynamics of the 15 February 2010 Maierato landslide (Calabria, Italy). Geomorphology 208:50–73. https://doi.org/10.1016/j.geomorph.2013.11.015

Borrelli L, Perri F, Critelli S, Gullà G (2014b) Characterization of granitoid and gneissic weathering profiles of the Mucone River basin (Calabria, southern Italy). Catena 113:325–340. https://doi.org/10.1016/j.catena.2013.08.014

Borrelli L, Cofone G, Coscarelli R, Gullà G (2015a) Shallow landslides triggered by consecutive rainfall events at Catanzaro strait (Calabria-Southern Italy). J Maps 11(5):730–744. https://doi.org/10.1080/17445647.2014.943814

Borrelli L, Coniglio S, Critelli S, La Barbera A, Gullà G (2015b) Weathering grade in granitoid rocks: the San Giovanni in Fiore area (Calabria, Italy). J Maps 12(2):260–275

Borrelli L, Critelli S, Gullà G, Muto F (2015c) Weathering grade and geotectonics of the western-central Mucone River basin (Calabria, Italy). J Maps 11(4):606–624. https://doi.org/10.1080/17445647.2014.933719

Brand EW, Phillipson HB (1985) Sampling and testing of residual soils: a review of international practice. Technical committee on sampling and testing of residual soils. International Society for Soil Mechanics and Foundation Engineering Scorpion Press 1–194

Brunsden D (1985) Landslide types, mechanisms, recognition, identification. In: Morgan CS (ed) Landslides in the South Wales Coalfield, Proceedings Symposium. The Polytechnic of Wales, pp 19–28

Bui D, Pradhan B, Lofman O, Dick O (2012) Landslide susceptibility assessment in the Hoa Binh Province of Vietnam: a comparison of the Levenberg-Marquardt and Bayesian regularized neural networks. Geophys J R Astron Soc 171–172:12–29

Calcaterra D, Parise M (2010) Weathering in the crystalline rocks of Calabria, Italy, and relationships to landslides. In: Calcaterra D, Parise M (eds) Weathering as a predisposing factor to slope movements. Geol Soc Lond, Eng Geol Spec Publ 23:105–130

Calvello M, Ciurleo M (2016) Optimal use of thematic maps for landslide susceptibility assessment by means of statistical analyses: case study of shallow landslides in fine grained soils. In: Proc ISL 2016, Landslides and engineered slopes experience—theory and practice, Napoli, Italy, vol. 2. pp. 537–544 (ISBN: 978-1-138-02988-0)

Carrara A, Cardinali M, Guzzetti F, Reichenbach P (1995) GIS technology in mapping landslide hazard. In: Carrara A, Guzzetti F (eds) Geographical information systems in assessing natural hazards. Kluwer Academic Publishers, pp. 135–175. doi: https://doi.org/10.1007/978-94-015-8404-3_8

Cascini L (2008) Applicability of landslide susceptibility and hazard zoning at different scales. Eng Geol 102(3-4):164–177. https://doi.org/10.1016/j.enggeo.2008.03.016

Cascini L, Gullà G (1993) Caratterizzazione fisico-meccanica dei terreni prodotti dall'alterazione di rocce gneissiche. Riv Ital Geotec 2:125–147

Cascini L, Ciurleo M, Di Nocera S, Gullà G (2015) A new–old approach for shallow landslide analysis and susceptibility zoning in fine-grained weathered soils of southern Italy. Geomorphology 241:371–381. https://doi.org/10.1016/j.geomorph.2015.04.017
Cascini L, Ciurleo M, Di Nocera S (2017) Soil depth reconstruction for the assessment of the susceptibility to shallow landslides in fine-grained slopes. Landslides 14(2):459–471. https://doi.org/10.1007/s10346-016-0720-8
Chigira M, Ito E (1999) Characteristic weathering profiles as basic causes of shallow landslides. In: Yagi N, Yamagami T, Jiang JC (eds) Slope Stability Engineering, vol 2. Balkema, Rotterdam, pp 1145–1150
Chigira M, Mohamad Z, Sian LC, Komoo I (2011) Landslides in weathered granitic rocks in Japan and Malaysia. Bull Geol Soc Malaysia 57:1–6
Chiu CF, Ng CWW (2014) Relationships between chemical weathering indices and physical and mechanical properties of decomposed granite. Eng Geol 179:76–89. https://doi.org/10.1016/j.enggeo.2014.06.021
Ciurleo M, Calvello M, Cascini L (2016) Susceptibility zoning of shallow landslides in fine grained soils by statistical methods. Catena 139:250–264. https://doi.org/10.1016/j.catena.2015.12.017
Ciurleo M, Cascini L, Calvello M (2017) A comparison of statistical and deterministic methods for shallow landslide susceptibility zoning in clayey soils. Eng Geol 223:71–81. https://doi.org/10.1016/j.enggeo.2017.04.023
Conforti M, Robustelli G, Muto F, Critelli S (2012) Application and validation of bivariate GIS-based landslide susceptibility assessment for the Vitravo river catchment (Calabria, south Italy). Nat Hazards 61(1):127–141. https://doi.org/10.1007/s11069-011-9781-0
Corominas J, van Westen C, Frattini P, Cascini L, Malet JP, Fotopoulou S, Catani F, Van Den Eeckhaut M, Mavrouli O, Agliardi F, Pitilakis K, Winter MG, Pastor M, Ferlisi S, Tofani V, Hervás J, Smith JT (2014) Recommendations for the quantitative analysis of landslide risk. Bull Eng Geol Environ 73:209–263
Cucci L, Tertulliani A (2006) I terrazzi marini nell'area di Capo Vaticano (Arco Calabro): solo un record di sollevamento regionale o anche di deformazione cosismica? Ital J Quat Sci 1:89–101
Das I, Sahoo S, van Westen C, Stein A, Hack R (2010) Landslide susceptibility assessment using logistic regression and its comparison with a rock mass classification system, along a road section in the northern Himalayas (India). Geomorphology 114(4):627–637. https://doi.org/10.1016/j.geomorph.2009.09.023
Deere DU, Patton FD (1971) Slope stability in residual soils. Proceedings of the 4th Pan American Conference on Soil Mechanics and Foundation Engineering, San Juan, Puerto Rico, pp 87–170
Duncan JM (1992) State-of-the-art: static stability and deformation analysis. Stability and performance of slopes and embankments-II. Geotechnical Engineering Division Special Publication. Am Soc Civ Eng 31:222–266
Durgin PB (1977) Landslides and the weathering of granitic rocks. Geological Society of America. Rev Eng Geol 3:127–131
Esposito C, Scarascia-Mugnozza G, Trigila A, Finoia MG (2012) Susceptibility assessment of shallow landslides in the Messina province. In: Eberhardt E, Froese C, Turner AK, Leroueil S (eds) Landslides and engineered slopes. Protecting society through improved understanding, vol 1. CRC Press, Taylor & Francis, Banff, pp 825–830
Fairbridge RW (ed) (1968) The encyclopedia of geomorphology. Reinhold, New York, p 1295
Fell R, Corominas J, Bonnard C, Cascini L, Leroi E, Savage WZ, On behalf of the JTC-1 Joint Technical Committee on Landslides and Engineered Slopes (2008) Guidelines for landslide susceptibility, hazard and risk zoning for land-use planning. Eng Geol 102(3-4):85–98. https://doi.org/10.1016/j.enggeo.2008.03.022
Ferrari E, Caloiero T, Coscarelli R (2013) Influence of the North Atlantic Oscillation on winter rainfall in Calabria (southern Italy). Theor Appl Climatol 114(3-4):479–494. https://doi.org/10.1007/s00704-013-0856-6
Fookes PG, Dearman WR, Franklin JA (1971) Some engineering aspects of rock weathering. J Eng Geol 4(3):139–185. https://doi.org/10.1144/GSL.QJEG.1971.004.03.01
Fressard M, Thiery Y, Maquaire O (2014) Which data for quantitative landslide susceptibility mapping at operational scale: case study of the Pays d'Auge plateau hillslopes (Normandy, France). Nat Hazards Earth Syst Sci 14(3):569–588. https://doi.org/10.5194/nhess-14-569-2014
Gan JKM, Fredlund DG (1996) Shear strength characteristics of two saprolitic soils. Can Geotech J 33(4):595–609. https://doi.org/10.1139/t96-085-307
Gioffrè D, Moraci N, Borrelli L, Gullà G (2016) Numerical code calibration for the back analysis of debris flow runout in southern Italy. Rend Online Soc Geol Ital 21:534–536
Goodman RE, Shi G (1985) Block theory and its applications to rock engineering. Prentice Hall
Gullà G, Borrelli L, Greco R (2004) Weathering of rock-mass as possible characterizing factor of predisposition to slope instabilities. In: Proc. of the 9th international symposium on landslides, Rio de Janeiro, June 28–July 7, 2004, pp 103–108
Gullà G, Antronico L, Borrelli L, Caloiero T, Coscarelli R, Iovine G, Nicoletti PG, Pasqua AA, Petrucci O, Terranova O (2009) Indicazioni conoscitive e metodologiche connesse all'evento di dissesto idrogeologico dell'autunno-inverno 2008-2009 in Calabria. Geol Calabria 10:4–21
Gullà G, Aceto L, Borrelli L (2012) Terreni di alterazione da rocce cristalline. Rend Online Soc Geol Ital 21:548–550
Guzzetti F, Mondini AC, Cardinali M, Fiorucci F, Santangelo M, Chang KT (2012) Landslide inventory maps: new tools for and old problem. Earth Sci Rev 112(1-2):42–66. https://doi.org/10.1016/j.earscirev.2012.02.001
Heidari M, Khanlari GR, Momeni AA, Jafargholizadeh H (2011) The relationship between geomechanical properties and weathering indices of granitic rocks, Hamedan, Iran. Geomech Geoeng 6(1):59–68. https://doi.org/10.1080/17486021003706580
Ietto F (2012) Cause dell'evento alluvionale del 19 ottobre 2010 nel bacino del Torrente delle Grazie (Tropea, Calabria). In: Proc Conference "Il Dissesto Idrogeologico: il pericolo geoidrologico e la gestione del territorio in Italia", Roma, pp 195–199
Ietto A, Calcaterra D (1988) Deformazioni gravitative profonde e tettonica presso Tropea (M.te Poro, Calabria). Mem Soc Geol Ital 41:911–915
Ietto A, Ietto F (2004) Age and history of the weathering of granitoids in southern Calabria (Italy). Geogr Fis Din Quat 27:37–45
Ietto F, Perri F, Fortunato G (2015) Lateral spreading phenomena and weathering processes from the Tropea area (Calabria, southern Italy). Environ Earth Sci 73(8):4595–4608. https://doi.org/10.1007/s12665-014-3745-0
Ietto F, Perri F, Cella F (2017) Weathering characterization for landslides modeling in granitoid rock masses of the Capo Vaticano promontory (Calabria, Italy). Landslides 15(1):1–20. https://doi.org/10.1007/s10346-017-0860-5
Irfan TY, Dearman WR (1978) The engineering petrography of a weathered granite in Cornwall, England. Q J Eng Geol 11:223–244
Jenks GF (1977) Optimal data classification for choropleth maps. In: Geography Department Occasional Paper No. 22. University of Kansas, Lawrence, KS, pp 1977
Kayastha P, Dhital MR, De Smedt F (2013) Evaluation of the consistency of landslide susceptibility mapping: a case study from the Kankai watershed in east Nepal. Landslides 10(6):785–799. https://doi.org/10.1007/s10346-012-0361-5
Kim MS, Onda Y, Uchida T, Kimd JK (2016) Effects of soil depth and subsurface flow along the subsurface topography. Geomorphology 271:40–54. https://doi.org/10.1016/j.geomorph.2016.07.031
Lacerda WA (2007) Landslide initiation in saprolite and colluvium in southern Brazil: field and laboratory observations. Geomorphology 87(3):104–119. https://doi.org/10.1016/j.geomorph.2006.03.037
Le Pera E, Sorriso-Valvo M (2000) Weathering and morphogenesis in a Mediterranean climate, Calabria, Italy. Geomorphology 34(3-4):251–270. https://doi.org/10.1016/S0169-555X(00)00012-X
Le Pera E, Critelli S, Sorriso-Valvo M (2001) Weathering of gneiss in Calabria, Southern Italy. Catena 42(1):1–15. https://doi.org/10.1016/S0341-8162(00)00117-X
Lee S, Chwae U, Min K (2002) Landslide susceptibility mapping by correlation between topography and geological structure: the Janghung area, Korea. Geomorphology 46(3-4):149–162. https://doi.org/10.1016/S0169-555X(02)00057-0
Lee C, Huang C, Lee J, Pan K, Lin M, Dong J (2008) Statistical approach to storm event-induced landslides susceptibility. Nat Hazards Earth Syst Sci 8(4):941–960. https://doi.org/10.5194/nhess-8-941-2008
Lumb P (1962) The properties of decomposed granite. Geotechnique 12(3):226–243. https://doi.org/10.1680/geot.1962.12.3.226
Marjanović (2013) Comparing the performance of different landslide susceptibility models in ROC space. In: Landslide science and practice. Volume 1: landslide inventory and susceptibility and hazard zoning pp 579–584
Metz CE (1978) Basic principles of ROC analysis. Semin Nucl Med 8(4):283–298. https://doi.org/10.1016/S0001-2998(78)80014-2
Nadim F, Einstein H, Roberds W (2005) Probabilistic stability analysis for individual slopes in soil and rock. State of the Art Report (SOA3). In: Hungr O, Fell R, Couture R, Eberhardt E (eds) Proceedings of the International Conference on "Landslide Risk Management", Vancouver (Canada). Taylor and Francis, London, pp 63–98
Nefeslioglu HA, Gokceoglu C, Sonmezb H (2008) An assessment on the use of logistic regression and artificial neural networks with different sampling strategies for the preparation of landslide susceptibility maps. Eng Geol 97(3-4):171–191. https://doi.org/10.1016/j.enggeo.2008.01.004
Nicotera P (1959) Rilevamento geologico del versante settentrionale del Monte Poro (Calabria). Mem Note Ist Geol Appl 7:1–92
Ollier C (1984) Weathering, 2nd edn. Longman, London 270
Ollier C (1988) The regolith in Australia. Earth Sci Rev 25(5-6):355–361. https://doi.org/10.1016/0012-8252(88)90003-7

Padrones JT, Ramos NT, Dimalanta CB, Queaño KL, Faustino-Eslava DV, Yumul GP, Watanabe K (2017) Landslide susceptibility mapping in a geologically complex terrane: a case study from northwest Mindoro, Philippines. Manila J Sci 10:25–44

Palacios D, Garcia R, Rubio V, Vigil R (2003) Debris flows in a weathered granitic massif: Sierra de gredos, Spain. Catena 51(2):115–140. https://doi.org/10.1016/S0341-8162(02)00094-2

Papazzoni C, Sirotti A (1999) Heterostegina Papyracea, Sequenza, 1880 from the upper Miocene of Cessaniti (Vibo Valentia, Calabria, southern Italy). Boll Soc Paleontol Ital 38:15–21

Perri F, Ietto F, Le Pera E, Apollaro C (2014) Weathering processes affecting granitoid profiles of Capo Vaticano (Calabria, southern Italy) based on petrographic, mineralogic and reaction path modelling approaches. Geol J 51:368–386

Santacana N, Baeza B, Corominas J, De Paz A, Marturia J (2003) A GIS-based multivariate statistical analysis for shallow landslide susceptibility mapping in La Pobla de Lillet Area (Eastern Pyrenees, Spain). Nat Hazards 30(3):281–295. https://doi.org/10.1023/B:NHAZ.0000007169.28860.80

Sato HP, Harp EL (2009) Interpretation of earthquake-induced landslides triggered by the 12 May 2008, M7.9 Wenchuan earthquake in the Beichuan area, Sichuan Province, China, using satellite imagery and Google Earth. Landslides 6(2):153–159. https://doi.org/10.1007/s10346-009-0147-6

Savage WZ, Godt JW, Baum RL (2004) Modelling time-dependent areal slope stability. In: Lacerda WA, Erlich M, Fontoura SAB, Sayao ASF (eds) Landslides: evaluation and stabilisation, Proceedings of the 9th international symposium on landslides. A.A. Balkema Publishers, London, pp 23–36

Scarciglia F, Critelli S, Borrelli L, Coniglio S, Muto F, Perri F (2016) Weathering profiles in granitoid rocks of the Sila Massif uplands, Calabria, southern Italy: new insights into their formation processes and rates. Sed Geol 336:46–67. https://doi.org/10.1016/j.sedgeo.2016.01.015

Soeters R, van Westen CJ (1996) Slope instability recognition, analysis and zonation. In: Turner AK, Schuster RL (eds) Landslides investigation and mitigation. TRB Special Report 247 National Academy Press, Washington D.C., pp 129–177

Steger S, Brenning A, Bell R, Glade T (2017) The influence of systematically incomplete shallow landslide inventories on statistical susceptibility models and suggestions for improvements. Landslides 14(5):1767–1781. https://doi.org/10.1007/s10346-017-0820-0

Sujatha ER, Rajamanickam GV, Kumaravel P (2012) Landslide susceptibility analysis using probabilistic certainty factor approach: a case study on Tevankarai stream watershed, India. J Earth Syst Sci 121:1337–1350

Swets JA (1988) Measuring the accuracy of diagnostic systems. Science 240(4857):1285–1293. https://doi.org/10.1126/science.3287615

Tangestani MH (2009) A comparative study of Dempster-Shafer and fuzzy models for landslide susceptibility mapping using a GIS: an experience from Zagros Mountains, SW Iran. J Asian Earth Sci 35(1):66–73. https://doi.org/10.1016/j.jseaes.2009.01.002

Tobe H, Chigira M (2006) Causes of shallow landslides of weathered granitic rocks—from the view point of weathering styles and petrologic textures. Disaster Mitigation of Debris Flows, Slope Failures and Landslides, Universal Academy Press, Inc./Tokyo, Japan, pp 493–501

Tortorici L, Monaco C, Tansi C, Cocina O (1995) Recent and active tectonics in the Calabrian arc (Southern Italy). Tectonophysics 243(1-2):37–55. https://doi.org/10.1016/0040-1951(94)00190-K

Tortorici G, Bianca M, De Guidi G, Monaco C, Tortorici L (2003) Fault activity and marine terracing in the Capo Vaticano area (southern Calabria) during the middle–late Quaternary. Quat Int 101:269–278

van Westen CJ (1994) GIS in landslide hazard zonation: a review, with examples from the Andes of Colombia. In: Price MF, Heywood DI (eds) Mountain environments and geographic information systems. Taylor and Francis Publishers, pp 135–165

Whalley WB, Turkington AV (2001) Weathering and geomorphology. Geomorphology 41(1):1–3. https://doi.org/10.1016/S0169-555X(01)00099-X

Yin KJ, Yan TZ (1988) Statistical prediction model for slope instability of metamorphosed rock. In: Proc. 5th Int Symposium on Landslides (Lausanne, Switzerland) vol 2l:1269–1272

L. Borrelli (✉) · **G. Gullà**
National Research Council of Italy—Research Institute for Geo-Hydrological Protection (CNR-IRPI),
Via Cavour 4/6, 87036, Rende, Cosenza, Italy
Email: luigi.borrelli@irpi.cnr.it

M. Ciurleo
Department of Civil Engineering,
University of Salerno,
Via Giovanni Paolo II, 132, 84084, Fisciano, Salerno, Italy